ACS OMEGA

http://pubs.acs.org/journal/acsodf

Article

Exploration of Converting Food Waste into Value-Added Products via Insect Pretreatment-Assisted Hydrothermal Catalysis

Ouyang Li, Jiaming Liang, Yundan Chen, Siqi Tang,* and Zhenshan Li*

Cite This: *ACS Omega* 2023, 8, 18760−18772

Read Online

ACCESS | Metrics & More | Article Recommendations | Supporting Information

ABSTRACT: The environmental burden of food waste (FW) disposal coupled with natural resource scarcity has aroused interest in FW valorization; however, transforming FW into valuable products remains a challenge because of its heterogeneous nature. In this study, a two-stage method involving black soldier fly (BSF)-based insect pretreatment and subsequent hydrothermal catalysis over a single-atom cerium-incorporated hydroxyapatite (Ce-HAP) was explored to convert FW into high added-value furfurals (furfural and 5-hydroxymethylfurfural). FW consisting of cereal, vegetables, meat, eggs, oil, and salt was initially degraded by BSF larvae to generate homogeneous BSF biomass, and then, crucial parameters impacting the conversion of BSF biomass into furfurals were investigated. Under the optimized conditions, 9.3 wt % yield of furfurals was attained, and repeated trials confirmed the recyclability of Ce-HAP. It was proved that the revenue of furfural production from FW by this two-stage method ranged from 3.14 to 584.4 USD/tonne. This study provides a potential technical orientation for FW resource utilization.

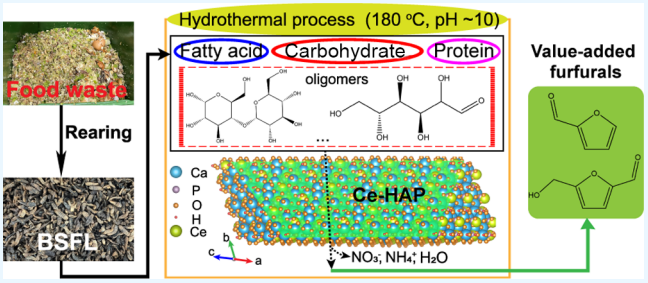

1. INTRODUCTION

The generation of food waste (FW) has increased as the global population and economy have grown. The 2021 World Economic Forum reports show that 931 million tons of FW are generated annually.[1] The vast amounts of FW are becoming a major environmental and economic burden because traditional FW treatments cannot meet sustainable development goals.[2] For example, composting has the advantages of low cost, easy operation, and high recovery efficiency,[3] while it generates greenhouse gases and leachate, and the economic benefits provided by FW compost are relatively poor.[4] Moreover, anaerobic digestion (AD) can produce considerable amounts of biogas as a source of energy,[5] but it does not harness the full potential of FW and produces harmful odors.[6] Consequently, according to the Sustainable Development Goals of Agenda 2030, the waste management of FW should be prioritized for production of high value chemicals over the formation of compost and bioenergy.[7,8]

The composition of food waste varies by source, region, climate, season, and culture of the country.[9] In America, FW is mainly composed of 30% vegetables and fruit, 21% pasta and bread, and 32% egg and milk, while in Asia, FW is composed of 56% vegetables and fruits, 34% rice and noodle, and around 4% egg and milk.[10] FW has been considered as the substrate to produce valuable chemicals (e.g., biosurfactants, biopolymers, diols);[7] however, it consists of waste flour, meat, eggs, vegetables, fruits, rice, oil, and salt[11] that exhibit high heterogeneity with diverse compositions of proteins, lipids, cellulose, hemicellulose, lignin, organic acids, vitamins, and minerals.[12,13] Therefore, it is difficult to transform FW directly into value-added products due to its complex components.

Taking composting and anaerobic digestion as examples, the abundant oil in FW limits the organic matter degradation and composting process by affecting the microbial community succession.[3] The protein and fat contained in FW are prone to lead to high ammonia concentration and long chain fatty acid in digestate after decomposition, resulting in low bioavailability and inhibition of the AD process.[14] As a result, it is necessary to adopt suitable pretreatment steps that are beneficial for improving the heterogeneous nature of FW before subsequent resource utilizations.

Various pretreatment methods are used for the isolation and extraction of FW, including physical, chemical, and biological processes.[15,16] For instance, Li et al. employed a three-stage pretreatment method of FW to achieve resource recovery, including freeze-drying for separating water, solvent exhaustion for extracting oil, and torrefaction to improve the properties of solid residue in FW to obtain a more coal-like solid product.[17] However, some organic ingredients (e.g., nitrogen, oxygen, and

Received: February 6, 2023
Accepted: May 9, 2023
Published: May 18, 2023

Table 1. Element and Component Analysis of Food Waste and BSF Biomass

sample name	element[a] (wt %, dry basis)					component[b] (wt %, dry basis)			
	C	H	N	S	O	protein	carbohydrate	lipid	ash[c]
food waste	46.5	6.9	3.2	0.4	35.3	16.1	50.9	15.2	6.0
BSF biomass	42.8	7.3	8.3	0.1	31.8	51.2	9.5	14.4	9.7

[a]The element analysis was detected by the CHNOS Elemental Analyzer (UNICUBE − Elementar). [b]The determination of proteins, lipids, and carbohydrates was measured according to the Chinese national standard GB 5009.5-2016, GB 5009.5-2016, and GB/T 15672-2009, respectively. [c]The ash content was determined through calcination in accordance with ASTM E1755-01.

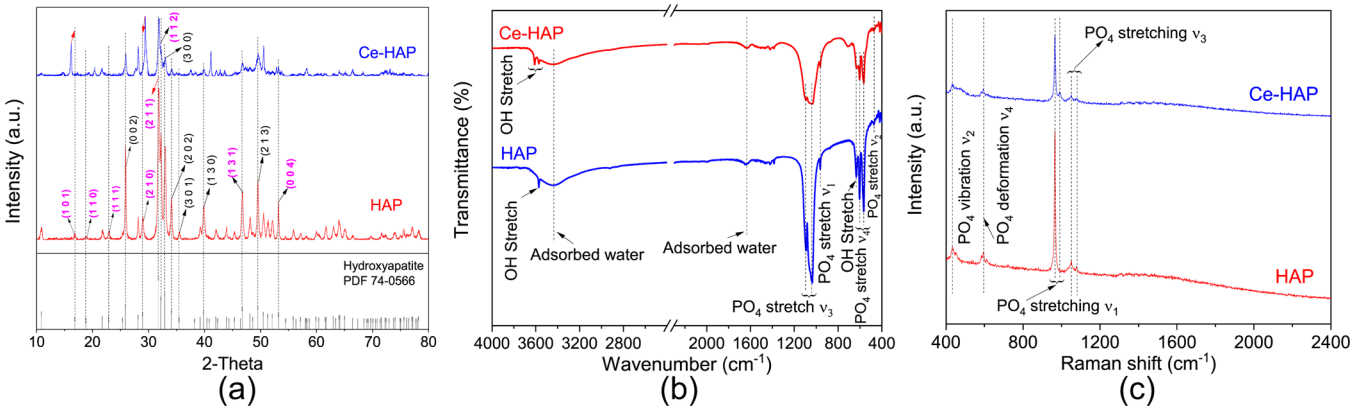

Figure 1. Basic structural characterizations of the synthesized Ce-HAP and HAP: (a) XRD patterns, (b) FT-IR spectra, and (c) Raman spectra.

phosphorus) in FW remain unutilized, and these pretreatment steps are complicated to generate a high capital input.

Recently, the emerging pretreatment based on insects has been adapted to change the heterogeneity of FW in an environmentally safe and cost-efficient manner.[18] As a human-benign insect, the black soldier fly (BSF) has displayed good competency in scavenging municipal organic wastes and assimilating them into insect biomass.[19,20] Importantly, it was demonstrated that the BSF larvae could survive from those heterogeneous components in FW, such as salts and oils,[21] and reduce the volume of FW by 80% in a short time.[22,23] Upon pretreatment, the obtained BSF biomass comprising proteins (37−63%), lipids (7−39%), and carbohydrates (8−20%) can be regarded as a valuable feedstock and applied for animal feed,[24,25] biodiesel production,[26] and chitin extraction.[27] It is noted that the constituents of BSF biomass may imply the possibility of other more valuable utilizations; however, to the best of our knowledge, related research is yet to be explored, particularly regarding the conversion of separate BSF biomass into value-added products.

In this study, a two-stage process involving insect pretreatment-assisted hydrothermal catalysis was explored to convert FW into value-added products. FW was first pretreated with BSF larvae and assimilated into the BSF biomass as feedstock. Cerium-incorporated hydroxyapatite (Ce-HAP) was synthesized via a one-pot hydrothermal process and used as the catalyst. During the catalytic process, the valuable platform compounds,[28,29] furfurals (furfural and 5-hydroxymethylfurfural) were produced and detected, as well as inorganic moieties (ammonium−nitrogen and nitrate−nitrogen). The influencing factors, including reaction temperature, reaction duration, catalyst loading, liquid-to-solid ratio, and initial solution pH, were investigated, and optimal conditions for furfural production and the removal of nitrogen-containing inorganics were obtained. Under optimized conditions, the recyclability of Ce-HAP was evaluated. This study offers a potential technical orientation for obtaining value-added products from FW through a two-stage method of suitable pretreatment followed by subsequent catalysis.

2. RESULTS AND DISCUSSION

2.1. Composition of the Obtained BSF Biomass. According to the results of the element and chemical composition analysis (Table 1), the initial material food waste contained C of 46.5%, H of 6.9%, O of 35.3%, N of 3.2%, and S of 0.4%, and the obtained biomass contained C of 42.8%, H of 7.3%, O of 31.8%, N of 8.3%, and S of 0.1%. The component analysis showed that the food waste mainly consisted of 16.1% proteins, 50.9% carbohydrates, 15.2% lipids, and 6.0% ash, and BSF biomass mainly consisted of 51.2% proteins, 9.5% carbohydrates, 14.4% lipids, and 9.7% ash.

The constituents involved were identified in detail for these general ingredients. In carbohydrate, 7 typical monosaccharide components, namely, glucose, fructose, lactose, maltose, ribose, arabinose, and xylose, were detected, and glucose had the highest content of 4.7% of the BSF biomass (Table S1). Among the 26 fatty acids identified in the BSF biomass (Table S2), oleic acid (4.8%), linoleic acid (4.0%), palmitic acid (3.1%), and dodecanoic acid (2.8%) were abundant in content. Meanwhile, 18 amino acids commonly consumed in human dietary life were found, the total of which occupied 48.38% of the BSF biomass (Table S3). Specifically, glutamic acid (6.0%), proline (4.4%), alanine (4.3%), histidine (4.0%), and aspartic acid (3.7%) were identified as the abundant species. Given that BSF biomass is rich in organic matter, exploratory trials are necessary to determine the resource utility of BSF biomass to value-added products such as furfurals.

2.2. Properties of the Synthesized Ce-HAP. Structural characterization of the synthesized Ce-HAP and pure HAP was conducted. As shown in Figure 1, X-ray diffraction (XRD) patterns showed that the introduction of Ce could alter the

https://doi.org/10.1021/acsomega.3c00762
ACS Omega 2023, 8, 18760−18772

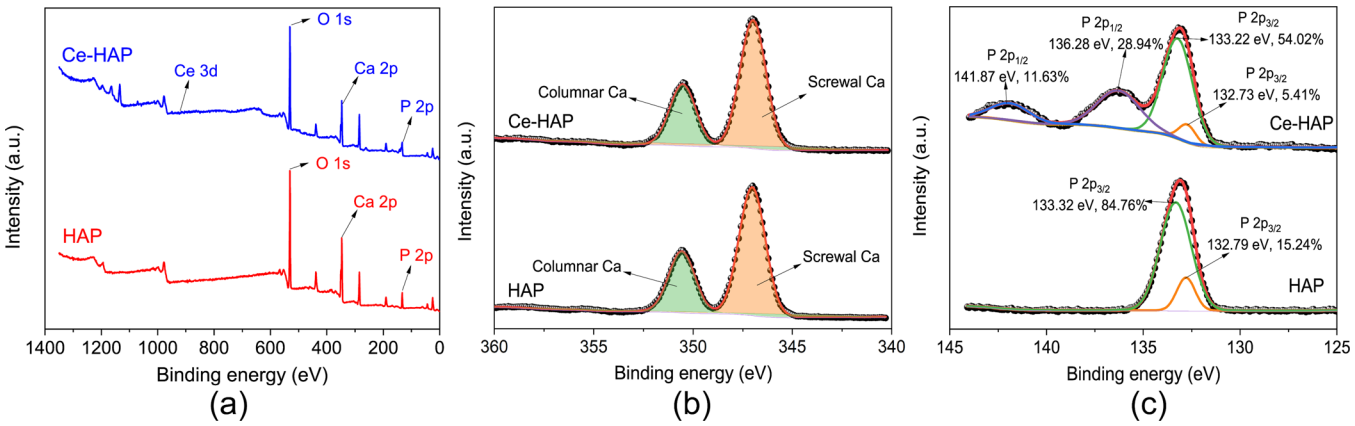

Figure 2. Basic structural characterizations of the synthesized Ce-HAP and HAP: (a) XPS surveys, (b) Ca 2p XPS spectra and the corresponding spectral deconvolutions, and (c) P 2p XPS spectra and the corresponding spectral deconvolutions.

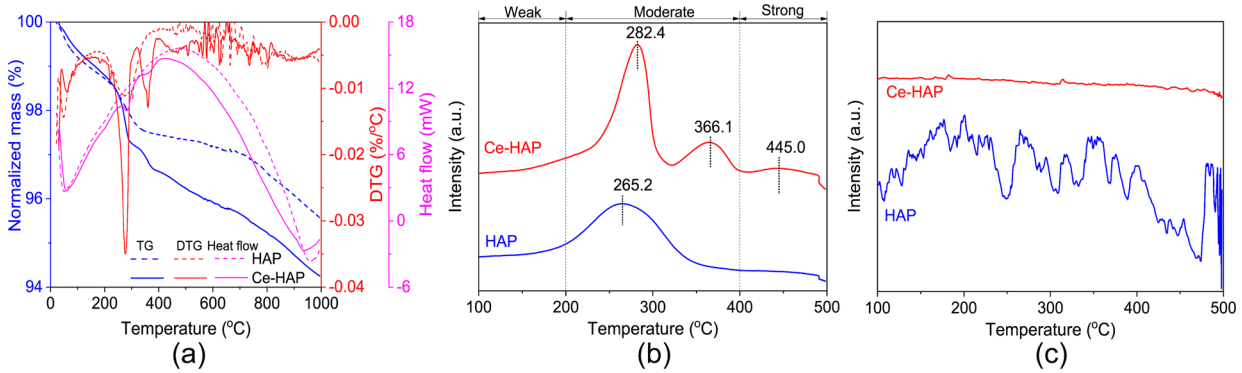

Figure 3. Basic structural characterizations of the synthesized Ce-HAP and HAP: (a) TG, DTG, and DTA curves, (b) CO_2-TPD curves, and (c) NH_3-TPD curves.

lattice orientation and atomic arrangements, as indicated by the intensity change on the Miller-indicated facets of (1 1 0), (1 1 1), (2 1 0), (1 1 2), (3 0 1), (1 3 1), and (0 0 4) on the HAP nanocrystals (Figure 1a). The shift toward decreased 2θ on (1 0 1) and (2 1 0) of Ce-HAP revealed that Ce incorporation modified the self-assembly process of HAP nanocrystals during synthesis. In contrast, the intensities of (1 0 1) and (2 1 0) became larger for Ce-HAP than those for pure HAP, suggesting that HAP lattice planes with a low-dimensional facet, such as (2 1 1), were preferentially incorporated by Ce atoms. The Fourier-transform infrared (FT-IR) spectra of Ce-HAP and pure HAP showed an analogous absorbance profile, indicating the formation of HAP nanoparticles (Figure 1b). The difference in the absorbance intensity induced by OH and PO_4 stretching between Ce-HAP and pure HAP suggests that the Ce atoms are embedded in the HAP nanocrystals. Congruent evidence for this statement was found in the Raman spectra (Figure 1c). The significantly decreased intensity at ~996 cm^{-1} indicative of the PO_4 stretching ν_1 mode indicated that the possible embedding positions of Ce atoms were near the space of P−O bands with the ν_1 stretching mode in the HAP lattice.[30]

The chemistry of building atoms in HAP lattices was elucidated using X-ray photoelectron spectroscopy (XPS) (Figure 2a). Two types of Ca atoms,[31] that is, screwal Ca (Ca(II)) centered at ~347.0 eV and columnar Ca (Ca(I)) centered at ~350.6 eV were clearly observed in the Ca 2p XPS spectrum (Figure 2b). The spectral convolutions showed that the two Ca atomic fractions were almost identical in Ce-HAP (Ca(I): Ca(II) being 31.74%:68.26%) and pure HAP (Ca-(I):Ca(II) being 31.66%:68.34%), indicating that the introduced Ce atoms could never neighbor the Ca atomic sites in HAP lattices. However, a noticeable difference was observed in the P 2p XPS spectrum (Figure 2c). One typical P state, i.e., P $2p_{3/2}$ with binding energies of 133.32 eV (84.76%) and 132.79 eV (15.24%), was found on the surface of HAP nanoparticles, which is in agreement with previous studies.[32,33] The presence of Ce atoms in the HAP lattice led to P chemical state splitting (P $2p_{3/2}$ and P $2p_{1/2}$), which further proved the above statements on the Ce atomic position in the HAP lattice in accordance with the Raman spectra.

Thermogravimetry (TG), derivative thermogravimetry (DTG), and differential thermal analysis (DTA) results of pure HAP and Ce-HAP are given in Figure 3a. Compared to pure HAP, Ce-HAP showed a larger weight loss over the entire temperature range and had more exposed hydroxyl groups (indicated by the abrupt peaks at ~277 and ~361 °C on the DTG curve).[34] The exceptional thermal stability of Ce-HAP demonstrated by its decomposition temperature (an analogous peak at 960 °C) underpinned its feasibility for practical catalytic applications. The temperature-programmed desorption of CO_2 (CO_2-TPD) (Figure 3b) and temperature-programmed desorption of NH_3 (NH_3-TPD) (Figure 3c) were conducted to investigate the catalytic site profiles of the prepared catalysts. The CO_2-TPD spectrum of pure HAP only showed a desorption peak centered at 265.2 °C (5.24 mmol/g), indicating that its basic strength was considered moderate.[35] This observation coincided with a higher molar

https://doi.org/10.1021/acsomega.3c00762
ACS Omega 2023, 8, 18760−18772

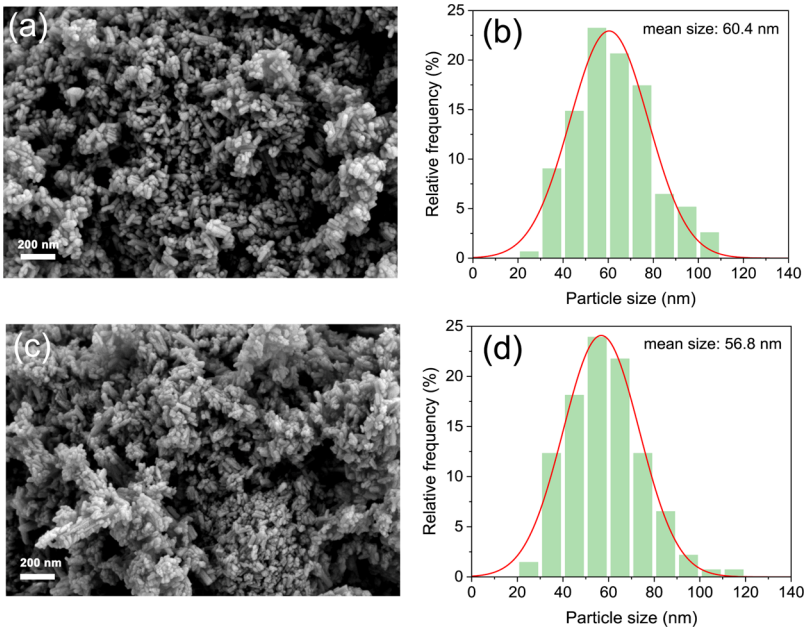

Figure 4. Electronic microscopy characterization: SEM images and the derived particle size distributions of (a, b) pure HAP and (c, d) Ce-HAP.

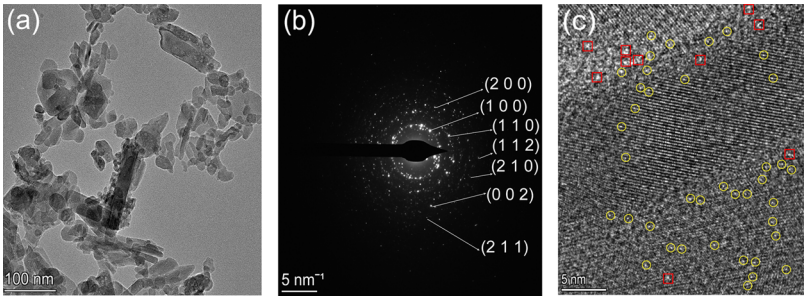

Figure 5. TEM images of Ce-HAP: (a) LRTEM, (b) SAED, and (c) HRTEM.

Ca/P ratio (1.71) than the stoichiometric ratio (1.67).[36] Three noticeable desorption peaks on the CO_2-TPD of Ce-HAP were centered at 282.4 °C (6.14 mmol/g), 366.1 °C (1.67 mmol/g), and 445.0 °C (0.99 mmol/g), and the total basicity density reached 7.81 mmol/g increasing by approximately 49% with regard to pure HAP. These TPD results explicitly demonstrate that the Ce atoms indeed strengthened the surface basicity of the HAP nanoparticles. Nevertheless, recognizable acid sites were difficult to find in the NH_3-TPD of Ce-HAP and pure HAP, suggesting that the dominant surface sites over Ce-HAP and pure HAP conferred basic catalysis.

To visualize the fine morphology of Ce-HAP and pure HAP, scanning electron microscopy (SEM) and transmission electron microscopy (TEM) were used to investigate their nanoscale dimensions. Notably, rodlike particles with longitudinal dimensional sizes in the nanoscale aggregated for pure HAP (Figure 4a), and the particle size distribution suggested a mean longitudinal length of approximately 60.4 nm (Figure 4b). An almost identical morphology was found in the SEM image of Ce-HAP (Figure 4c), with a mean longitudinal length of approximately 56.8 nm (Figure 4d). The crystal size of HAP decreased, and the refinement degree was about 6% after Ce doping. Correspondingly, combined with the changes of diffraction peak in XRD patterns, the introduction of Ce affected the self-assembly process of HAP nanocrystals in lattice space to a certain extent. Ce atoms would embed in gaps or lattice vacancies in the HAP lattice, which inhibited the local growth of HAP, and then, the finer nanostructures were formed. It means that the relative surface area of HAP nanocrystals was increased under the equal sample mass, which was conducive to the catalytic process.

The TEM images provide more detailed information on the inherent atomic architecture of Ce-HAP. The low-resolution TEM (LRTEM) image confirmed the rodlike morphology of the Ce-HAP nanoparticles (Figure 5a). The selected area electron diffraction (SAED) pattern depicted the orientation profile of the HAP lattice facets (Figure 5b), and these identified crystal planes with low Miller indices were typical in the HAP lattice.[37] The high-resolution TEM (HRTEM) image conferred a fine atomic arrangement (Figure 5c). The bright dots highlighted by yellow circles indicate the single-atom presence of Ce in HAP; meanwhile, minor aggregates of Ce atoms were marked by red rectangles (Figure S1). Moreover, two facets, (2 1 1) and (1 1 2), were recognized (Figure S2), which corresponded to the significant change in the peak intensities in the XRD pattern of Ce-HAP compared to that of pure HAP. To clearly elucidate the characteristics of the joint facets, a fast Fourier transform (FFT) on selected atomic configuration areas, followed by an inverse FFT, was performed on the HRTEM of Ce-HAP. It was determined that areas 1, 3, and 4, represented by red dashed rectangles, had well-crystallized arrangements, while the joint connections

https://doi.org/10.1021/acsomega.3c00762
ACS Omega 2023, 8, 18760−18772

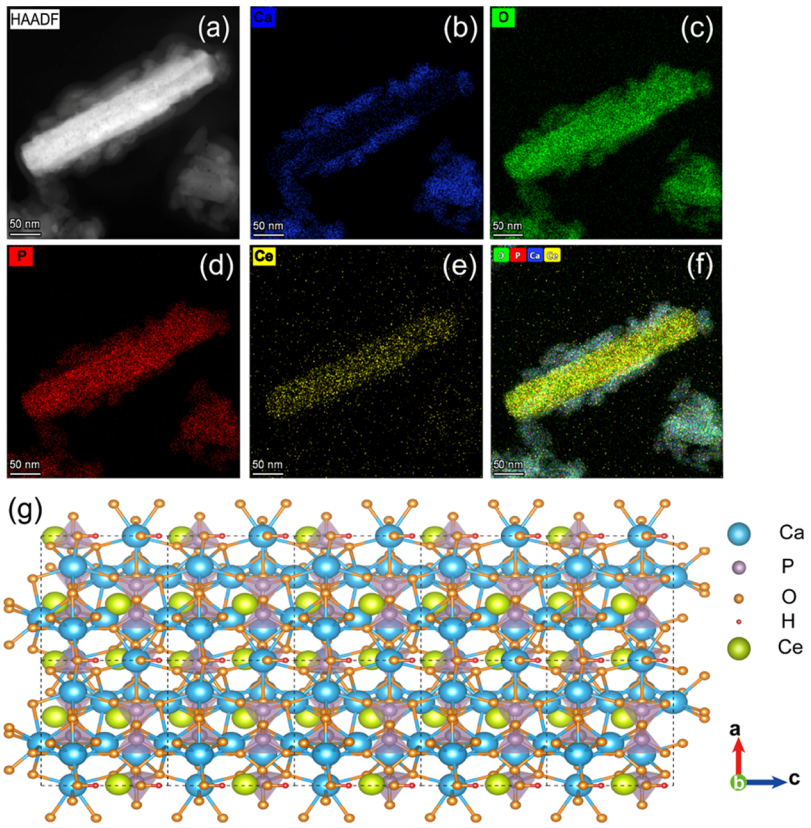

Figure 6. TEM images of Ce-HAP: (a) HAADF-STEM, (b–f) elemental (Ca, O, P, Ce) mappings, and (g) a constructed atomic configuration of Ce-HAP nanocrystals by the *b*-axis.

adjacent to facet (2 1 1), such as areas 2 and 5, showed a noticeable lattice dislocation. These findings confirmed that the Ce atoms were most likely to lie in the positions where the PO_4 groups stood at the joint planes adjacent to the facet (2 1 1).

The high angle angular dark field-scanning transmission electron microscopy (HAADF-STEM) image (Figure 6a) and elemental mapping (Figure 6b–f) illustrated the uniform spatial composition characteristic of the Ce-HAP nanocrystals. The low brightness of the Ce element and its distribution along the *c*-axis of the HAP lattice supported the presence of a single-atom Ce, which was in line with the determined Ce content (0.03%) by ICP-MS and that (0.03 at.%) by the Ce 3d XPS spectrum of Ce-HAP. Based on these electron microscopy analyses, an atomic-level configuration of Ce-HAP was conceived (Figure 6g).

2.3. Hydrothermal Catalytic Process of BSF Biomass over Ce-HAP. *2.3.1. Optimization of Furfural Production.* During the optimization of furfural production, hydrothermal temperature, reaction duration, catalyst loading, liquid-to-solid ratio, and initial solution pH were evaluated. The yield (Figure 7a) and selectivity (Figure 7b) of furfurals were selected as the target variables, as well as the nitrogen removal efficiency (NRE) (Figure 7c), defined as the conversion of organic nitrogen in the feedstock to ammonium–nitrogen (ammonium-N) and nitrate-nitrogen (nitrate-N), with the aim of decreasing the practical costs of purifying products. Other compounds belonging to aldehydes, ethers, nitrogenous compounds, phenols, ketones, and hydrocarbons were identified and analyzed (Figures S3–4, Table S4). The overall appearance of all the liquid samples obtained after the reaction was recorded (Figure S5).

It was found that an increase in the hydrothermal temperature improved the furfural yield and NRE. When the temperature was maintained at 140 °C, only 1.06 wt % of furfural yield and 36.72% of NRE were obtained. As the temperature increased to 180 °C, the furfural yield reached 8.09 wt % when an NRE increased up to 75.43%. This observation could be attributed to enhanced reaction kinetics at high temperatures.[38,39] When compared to undoped HAP (6.46 wt % furfural yield and 68.41% NRE), Ce-HAP outperformed in the catalytic conversion of BSF biomass to furfurals. Considering the highest product yield and NRE, the hydrothermal temperature of 180 °C was regarded as the desired reaction temperature. The reaction duration was optimized at the target temperature. When the reaction duration was held for 30 min, only 0.22 wt % furfurals were generated, with a product selectivity of 23.04% and an NRE of 10.96%. However, when the reaction duration was extended from 60 min up to 180 min, the furfural yield increased from 0.25 to 6.73 wt %, significantly increasing by 25.92%. When the reaction duration was extended up to 300 min, the furfural yields continually increased, i.e., 8.09 wt % and 48.83% of product selectivity and 75.43% of NRE. Because the three designated indicators were all higher than those in pure HAP catalysis, a reaction duration of 300 min was determined as desirable.

Notably, without a catalyst, aldehydes and nitrogenous compounds accounted for above 60% in those byproducts (Figure S4), and the organic acids and autohydrolysis reaction contributed only 1.5 wt % to the furfural production.[40,41] Thus,

https://doi.org/10.1021/acsomega.3c00762
ACS Omega 2023, 8, 18760–18772

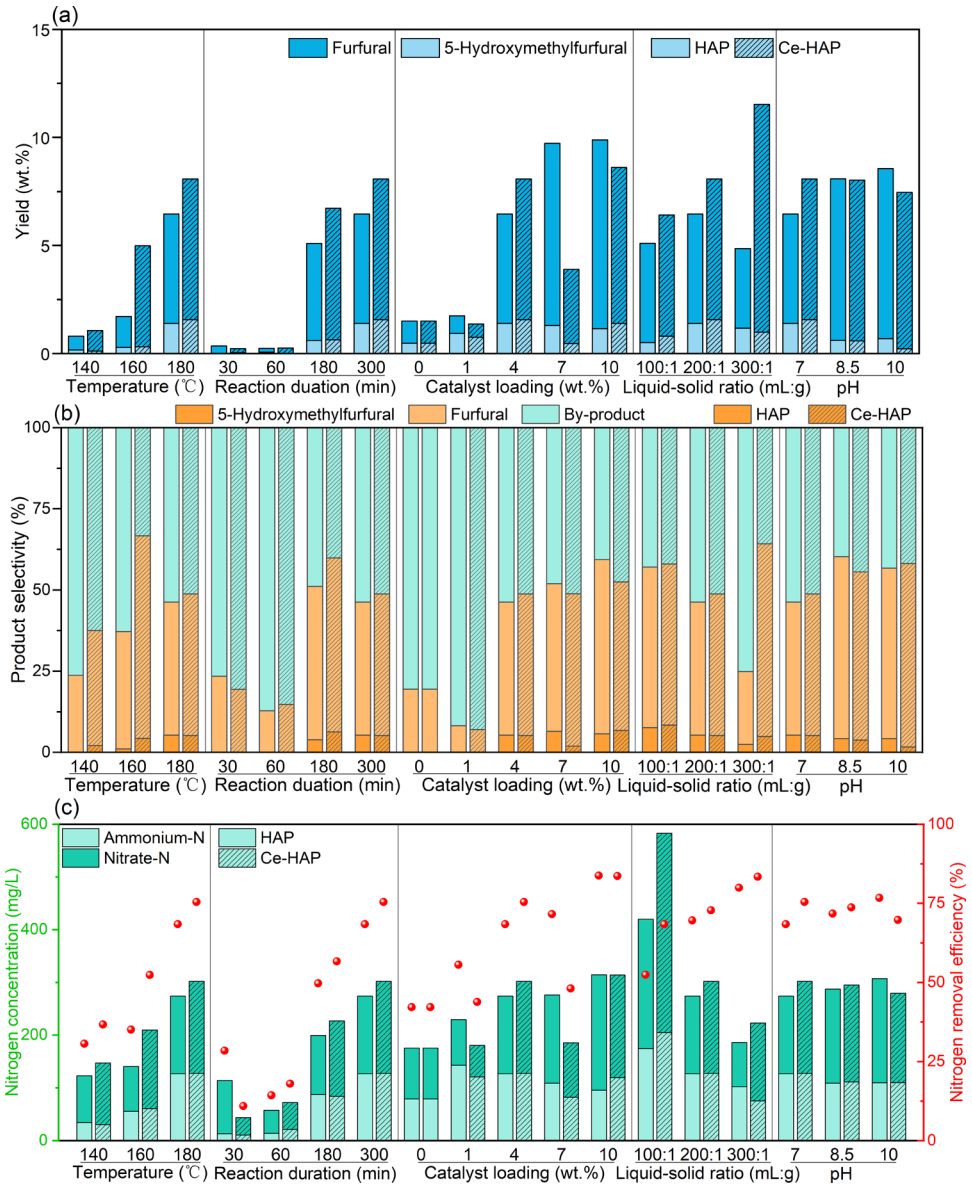

Figure 7. Effect of exploring conditions of furfural production in the hydrothermal catalytic process: (a) furfural yield, (b) product selectivity, and (c) inorganic nitrogen concentration (bar plot) and NRE.

the addition of a catalyst is indispensable for the conversion of BSF biomass to value-added furfurals. When the catalyst loading is maintained at 4 wt %, the product yield of furfurals reached 8.09 wt % with an NRE of 75.43%, and Ce-HAP was superior to pure HAP in these indicators. Although a further increase in catalyst loading to 10 wt % showed limited improvements in these indicators (8.61 wt % furfural yield and 83.69% NRE), the catalyst loading controlled at 4 wt % was desirable in terms of catalyst savings. In addition, the liquid-to-solid ratio affected furfural production during Ce-HAP catalysis, as evidenced by the significantly altered production of byproducts, such as aldehydes (Figure S4). When a low liquid-to-solid ratio of 100:1 was adopted, the substrate and obtained product compounds underwent various side reactions with each other.[42,43] Consequently, a 6.42 wt % furfural yield and 68.40% NRE were derived. As the ratio was further increased up to 300:1, the furfurals yield arrived at 11.53 wt % and the NRE was 83.45%, both higher than those for pure HAP. Therefore, a liquid-to-solid ratio of 300:1 was desirable for furfural production.

Finally, the influence of the pH was investigated. Previous studies have demonstrated that protecting HAP and its derived matrices from decomposition or ablation due to acids or acidic derivatives should maintain the reaction medium pH above 3.[44,45] In this study, without adjusting the pH of the initial solution, an 8.09 wt % furfural yield and 75.43% NRE were obtained, and the pH of the final liquid was 3.34 (Figure S6), which caused catalyst dissolution. When the initial solution pH was increased up to 10, the furfural yield was 7.46 wt % and the NRE was 69.75%, indicating that increased pH impaired the furfural yield. However, the final pH was 4.01 (Figure S6), suggesting that it can effectively protect Ce-HAP from structural damage.[46] Consequently, it is desirable to maintain the initial solution pH at 10.

Based on the above statements, the optimized reaction parameters were at 180 °C hydrothermal temperature, 300 min reaction duration, 4 wt % catalyst loading, 300:1 liquid−solid

https://doi.org/10.1021/acsomega.3c00762
ACS Omega 2023, 8, 18760−18772

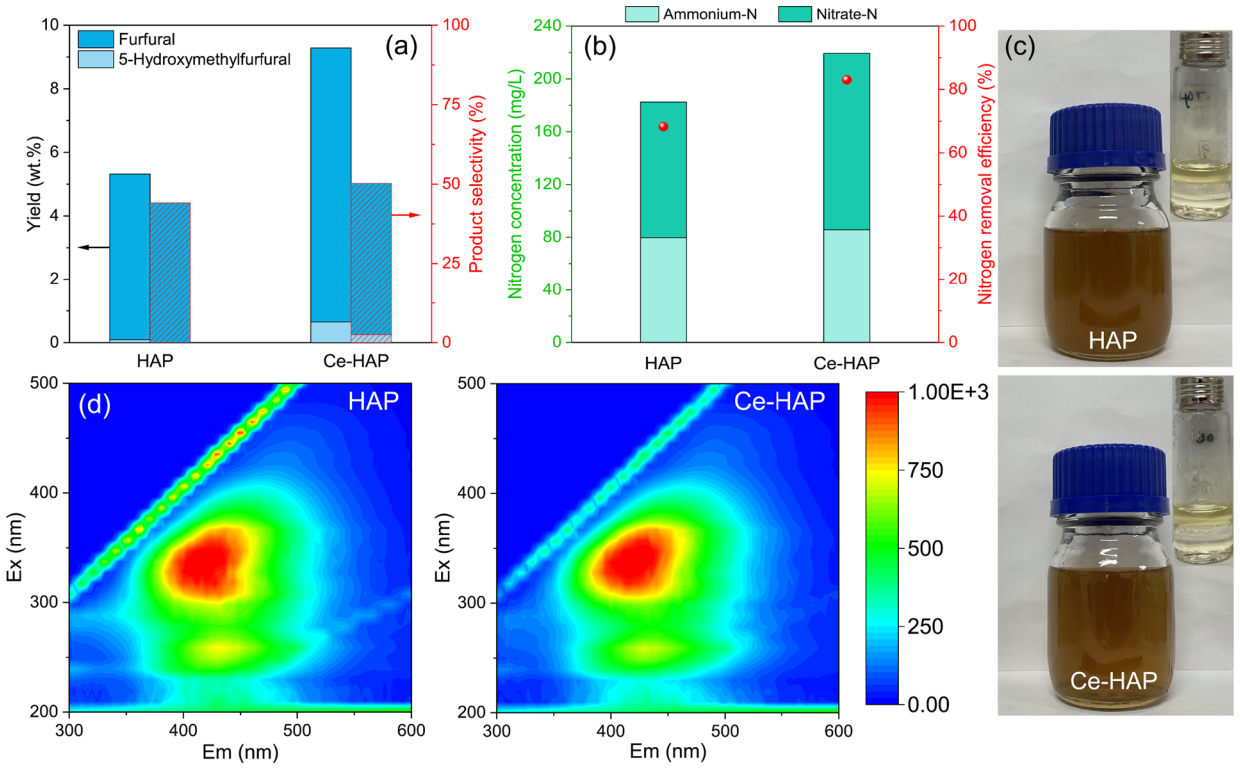

Figure 8. After deriving the optimum conditions, (a) the yield (left-vertical axis, bare bars) and product selectivity (right-vertical axis, shaded bars), (b) inorganic nitrogen concentrations (bar plot) and NRE, (c) apparent appearance (the inserted images at the right upper corner show the stratified liquids extracted by dichloromethane), and (d) 3D EEM spectra of the obtained liquids.

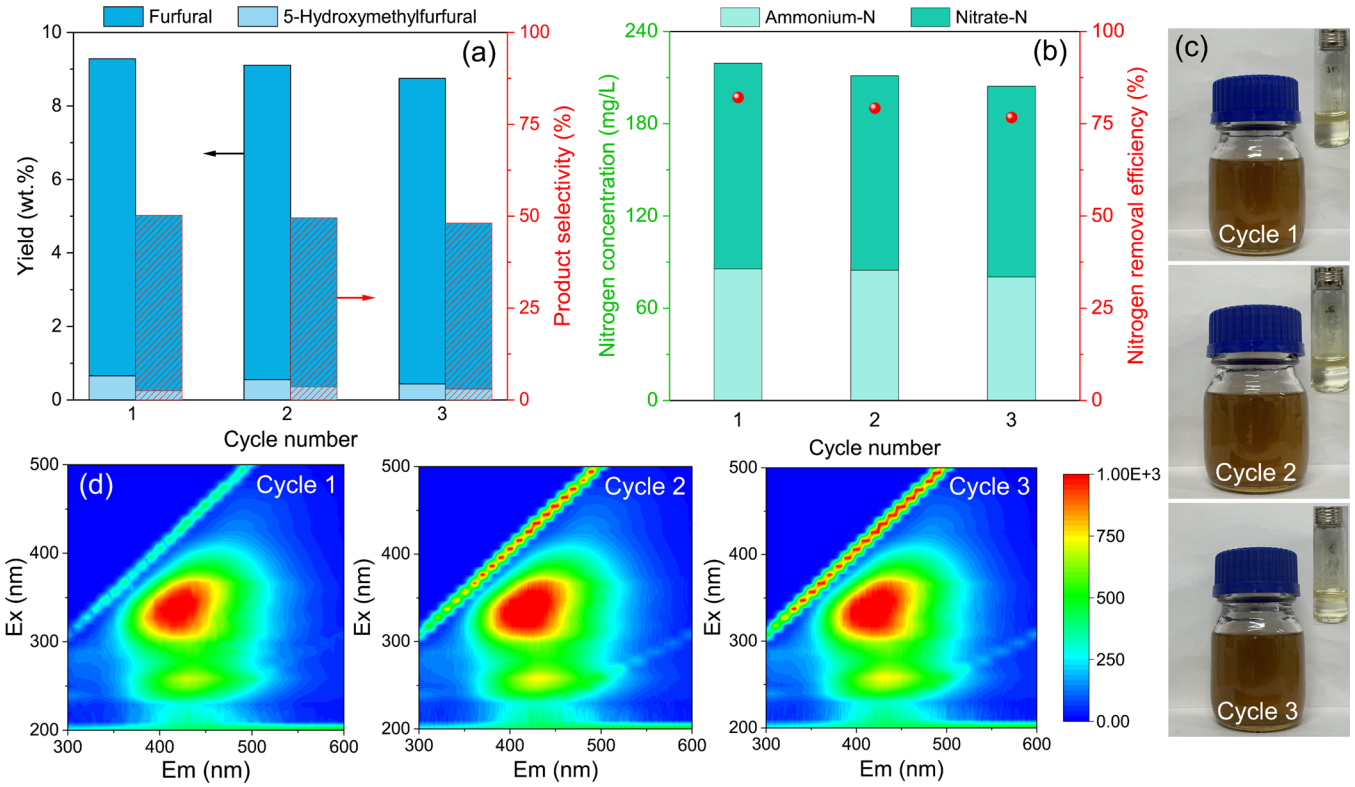

Figure 9. Recyclable performance of the Ce-HAP catalyst: (a) furfural yield (left-vertical axis, bare bars) and product selectivity (right-vertical axis, shaded bars), (b) inorganic nitrogen concentration (bar plot) and NRE, (c) apparent appearance, and (d) 3D EEM spectra of the obtained liquids.

ratio (mg/L), and initial solution of pH 10. Under the obtained optimized conditions, a 9.28 wt % furfural yield was realized in Ce-HAP catalysis, an increase of approximately 74% when compared to pure HAP (5.32 wt %), and the selectivity

https://doi.org/10.1021/acsomega.3c00762
ACS Omega 2023, 8, 18760−18772

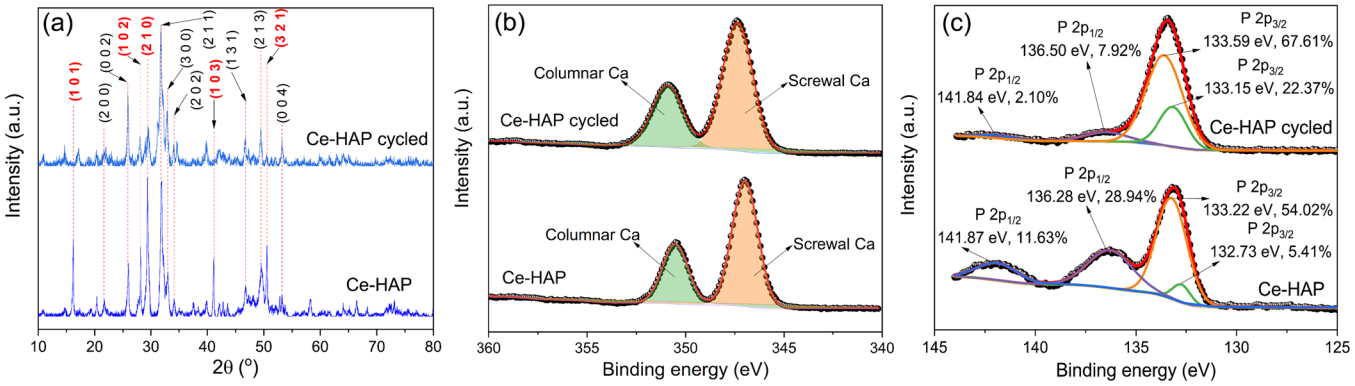

Figure 10. Recyclable performance of the Ce-HAP catalyst: (a) XRD patterns, (b) high-resolution Ca 2p XPS spectra, and (c) high-resolution P 2p XPS spectra.

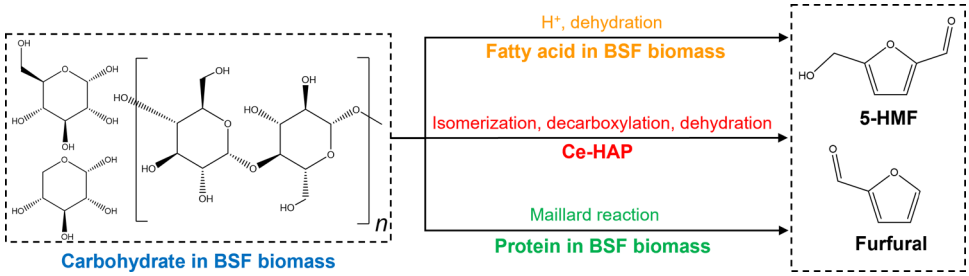

Figure 11. Proposed reaction pathways for the conversion of carbohydrates in the Ce-HAP catalytic system.

of furfurals was larger in Ce-HAP catalysis (50.3%) than in HAP catalysis (42.5%) (Figure 8a). Byproducts, including aldehydes, ethers, and nitrogenous compounds, generated from pure HAP were more abundant than those generated by Ce-HAP (Figure S7). As for the nitrogen-containing inorganic species, the nitrate-N and ammonium-N concentrations in the final liquid were determined to be 133.7 and 85.6 mg/L for Ce-HAP, respectively, which were both higher than those for HAP (102.6 and 79.8 mg/L, respectively). Thus, the NRE during Ce-HAP catalysis (83.1%) was higher than that during pure HAP catalysis (68.3%) (Figure 8b). From Figure 8c, it can be seen that the apparent color of the final liquid was dark brownish yellow either in pure HAP catalysis or Ce-HAP catalysis; however, the liquid after Ce-HAP catalysis showed a lighter color. This result confirms that there were more side reactions involving the production of humic substances during HAP catalysis.[47] In addition, the three-dimensional excitation-emission matrix (3D EEM) fluorescence spectra of the obtained liquids (Figure 8d) indicated a main absorption at emission >380 nm/excitation >250 nm contributed by heterocyclic oxygen and aldehyde groups,[48] possibly bearing the formation of furfurals.

2.3.2. Assessment of Ce-HAP Recyclability. To further evaluate the potential for the conversion of BSF biomass to value-added furfurals using the two-stage approach, the recyclability of Ce-HAP was examined. After three cycles, the production of aldehydes, phenols, and ethers in the byproducts tended to increase (Figure S7). As shown in Figure 9a, the furfural yield maintains at 8.75 wt %, reducing by only 5.71% with regard to the first cycle, and a similar trend of furfural selectivity is observed. Compared with the first cycle (82.1%), the NRE of biomass feedstock decreased slightly (76.6%) (Figure 9b). The almost identical apparent color of the obtained liquids (Figure 9c) and the corresponding 3D EEM fluorescence spectra (Figure 9d) demonstrated the stable performance of the catalyst, although a minor change in the recovered catalyst weight occurred after the cycle (Figure S8).

To probe the inherent changes in Ce-HAP after cycling, structural characterizations were performed on the recovered catalyst. Compared to the original Ce-HAP, the intensities of the ((1 0 1), (1 0 2), (2 1 0), (1 0 3), and (3 2 1)) facets showed various decreases in the XRD pattern of the cycled Ce-HAP (Figure 10a), suggesting that the catalytic sites located on these facets were likely to be deprived of the catalytic effect when Ce-HAP was repeatedly used. The pH of the final liquids decreased from 4.03 to 3.93, which may have affected the catalytic activity. In contrast, the (2 1 1) facet maintained almost identical intensities before and after cycling, revealing that the catalytic sites on this plane were responsible for the conversion. The Ca 2p XPS spectrum of the cycled Ce-HAP showed that 32.59% Ca(I) centered at ~350.9 eV and 67.41% Ca(II) centered at ~347.4 eV, both of which were identical to that for the fresh Ce-HAP (Figure 10b). This result indicates that the Ca atomic arrangements in the Ce-HAP lattice were stable during catalyst cycling. As mentioned in Section 2.2, the introduced Ce atoms were likely to locate the sites adjacent to the P atoms in the center of the PO_4 tetrahedron; thus, the P chemistry was anticipated to be most influenced during Ce-HAP cycling. Compared with the spinning state of P 2p chemistry over the fresh Ce-HAP, the fraction of the low-spin P $2p_{1/2}$ state significantly decreased, while that of the high-spin P $2p_{3/2}$ state significantly increased (Figure 10c). The Ce 3d XPS spectrum of cycled Ce-HAP had a profile similar to that of fresh Ce-HAP (Figure S9), and the Ce content of cycled Ce-HAP was 0.04 at.%, almost the same as that (0.03 at.%) of the fresh Ce-HAP. Thus, it is inferred that the Ce atoms anchored adjacent to P-centered tetrahedrons collectively catalyzed the conversion of ingredients in the BSF feedstock to furfurals.

https://doi.org/10.1021/acsomega.3c00762
ACS Omega 2023, 8, 18760−18772

Table 2. Revenue of Different FW Treatments

treatment	product	yield[a] (per tonne FW)	unit price of the product[b]	revenue[c] (USD/per tonne FW)	references
anaerobic digestion	biogas	65−420 m^3	0.11−0.40 USD/m^3	7.15−168 USD	(56−61)
aerobic composting	fertilizer	90−360 kg	0.04−0.48 USD/kg	3.6−172.8 USD	(56,62−66)
black soldier fly degradation	animal feed	30−105 kg[d]	0.33−5.60 USD/kg	9.9−588 USD	(67−72)
black soldier fly degradation	biodiesel	10−45 kg	0.6−1.2 USD/kg	6−54 USD	(26,73−77)
black soldier fly degradation	furfural and 5-hydroxymethylfurfural[e]	1.62 and 0.13 kg	1.7−120 and 3.0−3000 USD/kg[78−82]	3.14−584.4 USD	this study

[a]The yield of the product was obtained from 1 tonne FW. [b]The unit price of the product was determined based on the scale, purity, application, and the manufacturers from different regions. [c]The revenue range = yield (minimum) × price (minimum) to yield (maximum) × price (maximum). [d]The yield of animal feed was also inquired from the website (https://www.cgiar.org/research/publication/global-experiences-on-waste-processing-with-black-soldier-fly-hermetia-illucens-from-technology-to-business/). [e]The price of furfural and 5-HMF were also inquired from the website (https://www.chemicalbook.com/ProductList_En.aspx?kwd=HMF).

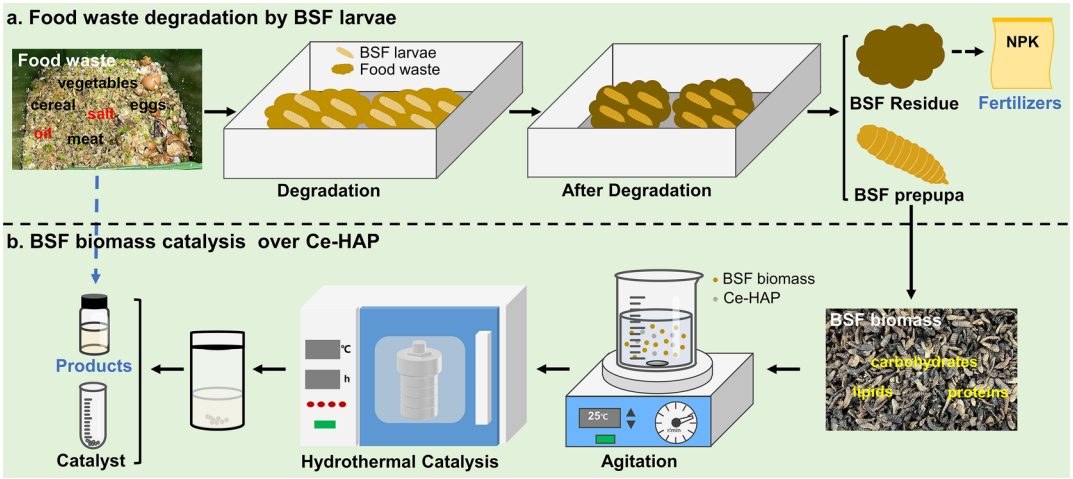

Figure 12. Schematic of the two-stage approach.

2.4. Reaction Pathways and Environmental Implications. In general, furfural is most derived from C5 sugars, but it can be produced through isomerization, decarboxylation, and dehydration,[49,50] when C6 sugars such as glucose were used as the substrate under the reaction conditions in this study (Figure S10). Accordingly, three possible reaction pathways for the catalytic conversion of BSF biomass to furfurals via Ce-HAP are proposed, as shown in Figure 11. Under the optimized reaction conditions, BSF biomass were first hydrolyzed to generate carbohydrates, fatty acids, and proteins. Fatty acids could provide the hydrogen ions capable of hydrolyzing and dehydrating carbohydrates, and amino acids could undergo the Maillard reaction with carbohydrates, which both produced furfurals.[51,52] Besides, the catalytic conversion of carbohydrates by Ce-HAP contributed to furfural production. As a versatile catalytic substrate, nanostructured HAP enabled the isomerization process of ketose-aldose, which was preferable for the reactions including dehydration, cyclization, and carbon−carbon bond cleavage.[53,54] As Figure 3b shows, the Ce atoms further augmented the surface basicity of the HAP nanoparticles. These strong basic sites distributed over Ce-HAP lay the foundation of its catalytic functionality, contributing to the key steps of furfural production, such as the isomerization and oriented cleavage of carbon−carbon bonds. Although Ca and Ce ions of Ce-HAP could induce hydrogen transfer and enhance the dehydration of carbohydrates, acidic sites should be modified in HAP to improve the furfural yield.[55]

The carbon balance analysis of the experiment (Figure S11) showed that 10.8% of the input carbon in the BSF biomass was accumulated in the solid residue, 18.3% was emitted to the atmosphere, and 70.9% passed to the liquid product (including 2.74% furfurals). In addition, the economic benefits of using the insect pretreatment-assisted two-stage hydrothermal catalysis approach to produce furfurals from FW were evaluated. In this study, 1.62 kg of furfural and 0.13 kg of 5-hydroxymethylfurfural could be obtained per tonne of FW under the optimal conditions. As shown in Table 2, the revenue range of FW using different valorization methods was calculated based on the yield and value of the products produced from each tonne of FW. It is found that the revenue of producing furfurals from FW was 3.14−584.4 USD/tonne through the two-stage method. Therefore, the developed two-stage method of BSF pretreatment-assisted Ce-HAP hydrothermal catalysis is a feasible strategy for valorizing FW in terms of producing the value-added products (furfural and 5-hydroxymethylfurfural).

3. CONCLUSIONS

A two-stage approach involving insect pretreatment-assisted hydrothermal catalysis was proposed to realize FW valorization. FW with complex compositions was first degraded by BSF larvae, and then, value-added furfurals (furfural and 5-

https://doi.org/10.1021/acsomega.3c00762
ACS Omega 2023, 8, 18760−18772

hydroxymethylfurfural) were generated from the carbohydrates in the obtained BSF biomass, using Ce-HAP as the catalyst. Under the optimized conditions, the furfural yield was 9.3 wt % and the Ce-HAP catalyst can be reused after regeneration. The revenue of producing furfurals using the two-stage method ranged from 3.14 to 584.4 USD/tonne of FW.

4. MATERIALS AND METHODS

A schematic of the insect pretreatment-assisted two-stage hydrothermal catalysis approach is shown in Figure 12, including FW degradation by BSF larvae and subsequent hydrothermal catalysis over Ce-HAP.

4.1. Insect Pretreatment of Food Waste by BSF Larvae. BSF (*Hermetia illucens*) eggs were purchased from a professional insect-breeding company in China. After 3-day hatching in a polyethylene-made plastic box (37 cm × 28 cm × 10 cm) filled with wheat bran, nascent BSF larvae were used to degrade the FW collected from a canteen at Peking University. The degradation process was performed in a polyethylene-made plastic box that was placed in a growth chamber operating at a relative humidity of 50% and curing temperature of 25 °C. When >90% of the larvae turned into prepupae,[83] the BSF prepupae were collected, washed, and cold-killed in a freezer (minus 20 °C). After lyophilization for 48 h, the dried BSF prepupae were ground into a powder as BSF biomass for subsequent experiments.

4.2. One-Pot Hydrothermal Synthesis of Ce-HAP. Ce-HAP was synthesized using a one-pot hydrothermal process. In brief, 8 mmol of calcium nitrate tetrahydrate ($Ca(NO_3)_2 \cdot 4H_2O$), 2 mmol of cerium nitrate hexahydrate ($Ce(NO_3)_3 \cdot 6H_2O$), and 6 mmol of potassium hydrogen phosphate dibasic ($K_2HPO_4 \cdot 3H_2O$) were dissolved in 150 mL of deionized water and magnetically mixed for 10 min. Subsequently, 28 mmol of potassium hydroxide (KOH) was added and magnetically stirred for another 10 min. Afterward, the solution was transferred to a 250-mL *p*-polyphenylene liner.[32] High-purity N_2 was used to purge the liner for 5 min before it was sealed in a stainless-steel autoclave. The autoclave was placed in an oven heated from 20 to 200 °C with a 24-h holding time. When the autoclave was naturally cooled, the solid product was collected by centrifugation (10,679 × *g*, 10 min) and then sequentially washed with ethanol and deionized water three times. Lyophilization was performed in a freeze-dryer (SJIA-10 N-50A, China) to obtain SAC Ce-HAP. For comparison, pure HAP was synthesized in the same manner as Ce-HAP, except that 8 mmol $Ca(NO_3)_2 \cdot 4H_2O$ and 2 mmol $Ce(NO_3)_3 \cdot 6H_2O$ were replaced with 10 mmol $Ca(NO_3)_2 \cdot 4H_2O$. The relevant characterization of the catalyst is provided in Text S1.

4.3. Production of Furfurals from BSF Biomass over Ce-HAP. The production of furfurals derived from the BSF feedstock was performed in a catalytic hydrothermal process over the prepared catalysts (Ce-HAP and HAP). Five predefined impactors, namely, hydrothermal temperature, reaction duration (holding for target temperature), catalyst loading, liquid-to-solid ratio between reactant and water, and initial solution (reaction medium) pH, were investigated. The detailed arrangement of the experimental trials is presented in Table S5. Typically, 500 mg of BSF powder and a predetermined amount of the catalyst (4 wt %) were added to a 250-mL beaker containing 156 mL of deionized water. The mixture was magnetically stirred for 30 min at 25 °C, and then, a 0.5 M KOH solution was used to adjust the initial solution pH to the target value (~10). Subsequently, the mixed solution was transferred to a stainless-steel autoclave equipped with a 250 mL polytetrafluorethylene liner. Prior to sealing, the liner was purged with a high-purity N_2 (99.999%, v/v) for 5 min. The autoclave was placed in a laboratory oven, heated to 180 °C, and maintained at this temperature for 300 min. When the heating procedure ended, the autoclave was naturally quenched. After centrifugation (10,679 × *g*, 8 min), the supernatant and solid in the liner were collected for further analysis. The analysis of the liquid sample and residual solids is detailed in Text S2.

4.4. Assessment of Catalyst Recyclability. Residual solids collected under optimal conditions were assessed for catalyst stability during repetitive assays. After lyophilization, the residual solid was calcined in a muffle furnace (500 °C, 4 h) to obtain the required catalyst for the next cycle. The amount of BSF biomass added was determined based on the optimized catalyst loading. The other operations on the hydrothermal reaction, liquid separation and detection, and residual solid collection and calcination were identical to those in the former trial. Furthermore, the catalyst obtained during the last cycle was collected for structural characterization.

■ ASSOCIATED CONTENT

Data Availability Statement

The data underlying this study are available in the published article and its Supporting Information. Extra data are available from the corresponding author upon request.

Supporting Information

The Supporting Information is available free of charge at https://pubs.acs.org/doi/10.1021/acsomega.3c00762.

Characterization methods of catalyst; qualitative and quantitative analyses of liquid samples; HRTEM of Ce-HAP; dislocation analysis of Ce-HAP; GC−MS spectrogram of liquid samples; mass spectrum analyses of byproducts; apparent appearance of liquid samples; pH of liquid samples; mass change of cycled Ce-HAP; Ce 3d XPS spectra of cycled Ce-HAP; analyses of byproducts under the optimum and recycled condition; GC−MS spectrogram of liquid samples after catalyzing glucose; carbon balance analysis in hydrothermal catalysis; standard curve for furfural measurement; carbohydrate monomers in BSF biomass; fatty acids in BSF biomass; amino acids in BSF biomass; identified compounds in liquid sample; and experimental plan (PDF)

■ AUTHOR INFORMATION

Corresponding Authors

Siqi Tang − *College of Environmental Sciences and Engineering, State Environmental Protection Key Laboratory of All Material Fluxes in River Ecosystems, Peking University, Beijing 100871, PR China;* orcid.org/0000-0001-6023-7294; Phone: +86 010-62753962; Email: siqitang@pku.edu.cn

Zhenshan Li − *College of Environmental Sciences and Engineering, State Environmental Protection Key Laboratory of All Material Fluxes in River Ecosystems, Peking University, Beijing 100871, PR China;* orcid.org/0000-0002-1110-3588; Phone: +86 010-62753962; Email: lizhenshan@pku.edu.cn

https://doi.org/10.1021/acsomega.3c00762
ACS Omega 2023, 8, 18760−18772

Authors

Ouyang Li − *College of Environmental Sciences and Engineering, State Environmental Protection Key Laboratory of All Material Fluxes in River Ecosystems, Peking University, Beijing 100871, PR China*

Jiaming Liang − *College of Environmental Sciences and Engineering, State Environmental Protection Key Laboratory of All Material Fluxes in River Ecosystems, Peking University, Beijing 100871, PR China*

Yundan Chen − *College of Environmental Sciences and Engineering, State Environmental Protection Key Laboratory of All Material Fluxes in River Ecosystems, Peking University, Beijing 100871, PR China*

Complete contact information is available at: https://pubs.acs.org/10.1021/acsomega.3c00762

Author Contributions

All authors contributed to the study conception and design. Conceptualization, investigation, data curation, and formal analysis were performed by O.L., S.T., and J.L. The first draft of the manuscript was written by O.L. The revision and edition of the manuscript were performed by S.T., J.L., Y.C., and Z.L. Funding acquisition and supervision were performed by S.T. and Z.L.

Notes

The authors declare no competing financial interest.

■ ACKNOWLEDGMENTS

This research was financially supported by the National Key Research and Development Program of China (grant number 2022YFC3201801) and the National Natural Science Foundation of China (grant number 32202605).

■ REFERENCES

(1) Roy, P.; Mohanty, A. K.; Dick, P.; Misra, M. A Review on the Challenges and Choices for Food Waste Valorization: Environmental and Economic Impacts. *ACS Environ. Au* **2023**, *3*, 58−75.

(2) Jeevahan, J.; Anderson, A.; Sriram, V.; Durairaj, R. B.; Britto Joseph, G.; Mageshwaran, G. Waste into Energy Conversion Technologies and Conversion of Food Wastes into the Potential Products: A review. *Int. J. Ambient Energy* **2021**, *42*, 1083−1101.

(3) Liu, J.; Shen, Y.; Ding, J.; Luo, W.; Zhou, H.; Cheng, H.; Wang, H.; Zhang, X.; Wang, J.; Xu, P.; Cheng, Q.; Ma, S.; Chen, K. High Oil Content Inhibits Humification in Food Waste Composting by Affecting Microbial Community Succession and Organic Matter Degradation. *Bioresour. Technol.* **2023**, *376*, No. 128832.

(4) Sridhar, A.; Kapoor, A.; Kumar, P. S.; Ponnuchamy, M.; Balasubramanian, S.; Prabhakar, S. Conversion of Food Waste to Energy: A Focus on Sustainability and Life Cycle Assessment. *Fuel* **2021**, *302*, No. 121069.

(5) Elgarahy, A. M.; Eloffy, M. G.; Alengebawy, A.; El-Sherif, D. M.; Gaballah, M. S.; Elwakeel, K. Z.; El-Qelish, M. Sustainable Management of Food Waste; Pre-Treatment Strategies, Techno-Economic Assessment, Bibliometric Analysis, and Potential Utilizations: A Systematic Review. *Environ. Res.* **2023**, *225*, No. 115558.

(6) Narisetty, V.; Cox, R.; Willoughby, N.; Aktas, E.; Tiwari, B.; Matharu, A. S.; Salonitis, K.; Kumar, V. Recycling Bread Waste into Chemical Building Blocks Using a Circular Biorefining Approach. *Sustainable Energy Fuels* **2021**, *5*, 4842−4849.

(7) Narisetty, V.; Adlakha, N.; Kumar Singh, N.; Dalei, S. K.; Prabhu, A. A.; Nagarajan, S.; Naresh Kumar, A.; Amruthraj Nagoth, J.; Kumar, G.; Singh, V.; Kumar, V. Integrated Biorefineries for Repurposing of Food Wastes into Value-Added Products. *Bioresour. Technol.* **2022**, *363*, No. 127856.

(8) Kammen, D. M.; Sunter, D. A. City-Integrated Renewable Energy for Urban Sustainability. *Science* **2016**, *352*, 922−928.

(9) Chhandama, M. V. L.; Chetia, A. C.; Satyan, K. B.; Supongsenla, A.; Ruatpuia, J. V. L.; Rokhum, S. L. Valorisation of Food Waste to Sustainable Energy and Other Value-Added Products: A Review. *Bioresour. Technol. Rep.* **2022**, *17*, No. 100945.

(10) Braguglia, C. M.; Gallipoli, A.; Gianico, A.; Pagliaccia, P. Anaerobic Bioconversion of Food Waste into Energy: A Critical Review. *Bioresour. Technol.* **2018**, *248*, 37−56.

(11) Ma, C. N.; Liu, J. Y.; Ye, M.; Zou, L. P.; Qian, G. R.; Li, Y. Y. Towards Utmost Bioenergy Conversion Efficiency of Food Waste: Pretreatment, Co-Digestion, and Reactor Type. *Renew. Sustain. Energy Rev.* **2018**, *90*, 700−709.

(12) Alibardi, L.; Astrup, T. F.; Asunis, F.; Clarke, W. P.; De Gioannis, G.; Dessi, P.; Lens, P. N. L.; Lavagnolo, M. C.; Lombardi, L.; Muntoni, A.; Pivato, A.; Polettini, A.; Pomi, R.; Rossi, A.; Spagni, A.; Spiga, D. Organic Waste Biorefineries: Looking towards Implementation. *Environ. Sci. Pollut. Res.* **2020**, *114*, 274−286.

(13) Tirapanampai, C.; Toewiwat, N.; Weeranoppanant, N.; Chaiyen, P.; Wongnate, T. Processing of Palm Oil Mill Effluent (POME) into Food Waste Digesting Microbes: An Investigation of Acclimatization Strategies. *Sustain. Energy Technol.* **2022**, *52*, No. 102287.

(14) Wang, L.; Zhu, L.; Pan, S.; Wang, S. Low-Carbon Emitting University Campus Achieved via Anaerobic Digestion of Canteen Food Wastes. *J. Environ. Manage.* **2023**, *335*, No. 117533.

(15) Ferdes, M.; Zabava, B. S.; Paraschiv, G.; Ionescu, M.; Dinca, M. N.; Moiceanu, G. Food Waste Management for Biogas Production in the Context of Sustainable Development. *Energies* **2022**, *15*, 6268.

(16) Kumar, V.; Sharma, N.; Umesh, M.; Selvaraj, M.; Al-Shehri, B. M.; Chakraborty, P.; Duhan, L.; Sharma, S.; Pasrija, R.; Awasthi, M. K.; Lakkaboyana, S. R.; Andler, R.; Bhatnagar, A.; Maitra, S. S. Emerging Challenges for the Agro-Industrial Food Waste Utilization: A Review on Food Waste Biorefinery. *Bioresour. Technol.* **2022**, *362*, No. 127790.

(17) Li, R.; Gong, M. H.; Biney, B. W.; Chen, K.; Xia, W.; Liu, H.; Guo, A. J. Three-Stage Pretreatment of Food Waste to Improve Fuel Characteristics and Incineration Performance with Recovery of Process By-Products. *Fuel* **2022**, *330*, No. 125655.

(18) Ojha, S.; Bussler, S.; Schluter, O. K. Food Waste Valorisation and Circular Economy Concepts in Insect Production and Processing. *Waste Manage.* **2020**, *118*, 600−609.

(19) Purkayastha, D.; Sarkar, S. Black Soldier Fly Larvae for Treatment and Segregation of Commingled Municipal Solid Waste at Different Environmental Conditions. *J. Environ. Manage.* **2022**, *302*, No. 114060.

(20) Salam, M.; Shahzadi, A.; Zheng, H. L.; Alam, F.; Nabi, G.; Dezhi, S.; Ullah, W.; Ammara, S.; Ali, N.; Bilal, M. Effect of Different Environmental Conditions on the Growth and Development of Black Soldier Fly Larvae and Its Utilization in Solid Waste Management and Pollution Mitigation. *Environ. Technol. Innov.* **2022**, *28*, No. 102649.

(21) Ji, Y.; Ren, D.; Ye, M.; Xu, Q.; An, X. Tolerance of the Black Soldier Fly, Hermetia Illucens (Diptera: Stratiomyidae) to pH Value, Pungency, and NaCl in Foodstuffs. *Chin. J. Appl. Environ. Biol.* **2018**, *24*, 636−639.

(22) Palma, L.; Fernandez-Bayo, J.; Niemeier, D.; Pitesky, M.; VanderGheynst, J. S. Managing High Fiber Food Waste for the Cultivation of Black Soldier Fly Larvae. *NPJ Sci. Food* **2019**, *3*, 15.

(23) Kim, C. H.; Ryu, J.; Lee, J.; Ko, K.; Lee, J. Y.; Park, K. Y.; Chung, H. Use of Black Soldier Fly Larvae for Food Waste Treatment and Energy Production in Asian Countries: A Review. *Processes* **2021**, *9*, 161.

(24) Barragan-Fonseca, K. B.; Dicke, M.; van Loon, J. J. A. Nutritional Value of the Black Soldier Fly (Hermetia Illucens L.) and Its Suitability as Animal Feed − A Review. *J. Insects Food Feed* **2017**, *3*, 105−120.

(25) Panikkar, P.; Parakkandi, J.; Khan, F.; Das, B. K.; Udayakumar, A.; Eregowda, V. M.; Yandigeri, M. Use of Black Soldier Fly (Hermetia Illucens) Prepupae Reared on Organic Waste as Feed or as

an Ingredient in a Pellet-Feed Formulation for Nile Tilapia (Oreochromis Niloticus). *Environ. Sci. Pollut. Res.* **2022**, *29*, 72968−72978.
(26) Jung, S.; Jung, J. M.; Tsang, Y. F.; Bhatnagar, A.; Chen, W. H.; Lin, K. Y. A.; Kwon, E. E. Biodiesel Production from Black Soldier Fly Larvae Derived from Food Waste by Non-Catalytic Transesterification. *Energy* **2022**, *238*, No. 121700.
(27) Surendra, K. C.; Tomberlin, J. K.; van Huis, A.; Cammack, J. A.; Heckmann, L. H. L.; Khanal, S. K. Rethinking Organic Wastes Bioconversion: Evaluating the Potential of the Black Soldier Fly (Hermetia Illucens (L.)) (Diptera: Stratiomyidae) (BSF). *Waste Manage.* **2020**, *117*, 58−80.
(28) Gabriel, J. B.; Oliveira, V.; de Souza, T. E.; Padula, I.; Oliveira, L. C. A.; Gurgel, L. V. A.; Baeta, B. E. L.; Silva, A. C. New Approach to Dehydration of Xylose to 2-Furfuraldehyde Using a Mesoporous Niobium-Based Catalyst. *ACS Omega* **2020**, *5*, 21392−21400.
(29) Vasishta, A.; Pawar, H. S. PolyE-IL Is an Efficient and Recyclable Homogeneous Catalyst for the Synthesis of 5-Hydroxymethyl Furfural in a Green Solvent. *ACS Omega* **2023**, *8*, 1047−1059.
(30) Londono-Restrepo, S. M.; Zubieta-Otero, L. F.; Jeronimo-Cruz, R.; Mondragon, M. A.; Rodriguez-Garcia, M. E. Effect of the Crystal Size on the Infrared and Raman Spectra of Bio Hydroxyapatite of Human, Bovine, and Porcine Bones. *J. Raman Spectrosc.* **2019**, *50*, 1120−1129.
(31) Astala, R.; Stottt, M. J. First-Principles Study of Hydroxyapatite Surfaces and Water Adsorption. *Phys. Rev. B* **2008**, *78*, No. 075427.
(32) Chernozem, R. V.; Surmeneva, M. A.; Krause, B.; Baumbach, T.; Ignatov, V. P.; Tyurin, A. I.; Loza, K.; Epple, M.; Surmenev, R. A. Hybrid Biocomposites Based on Titania Nanotubes and a Hydroxyapatite Coating Deposited by RF-Magnetron Sputtering: Surface Topography, Structure, and Mechanical Properties. *Appl. Surf. Sci.* **2017**, *426*, 229−237.
(33) Lopez, E. O.; Bernardo, P. L.; Checca, N. R.; Rossi, A. L.; Mello, A.; Ellis, D. E.; Rossi, A. M.; Terra, J. Hydroxyapatite and Lead-Substituted Hydroxyapatite Near-Surface Structures: Novel Modelling of Photoemission Lines from X-Ray Photoelectron Spectra. *Appl. Surf. Sci.* **2022**, *571*, No. 151310.
(34) Zhang, W.; Wang, F.; Wang, P.; Lin, L.; Zhao, Y.; Zou, P.; Zhao, M.; Chen, H.; Liu, Y.; Zhang, Y. Facile Synthesis of Hydroxyapatite/Yeast Biomass Composites and Their Adsorption Behaviors for Lead (II). *J. Colloid Interface Sci.* **2016**, *477*, 181−190.
(35) Haydar, S.; Moreno-Castilla, C.; Ferro-García, M. A.; Carrasco-Marín, F.; Rivera-Utrilla, J.; Perrard, A.; Joly, J. P. Regularities in the Temperature-Programmed Desorption Spectra of CO_2 and CO from Activated Carbons. *Carbon* **2000**, *38*, 1297−1308.
(36) Ibrahim, M.; Labaki, M.; Giraudon, J. M.; Lamonier, J. F. Hydroxyapatite, a Multifunctional Material for Air, Water and Soil Pollution Control: A review. *J. Hazard. Mater.* **2020**, *383*, No. 121139.
(37) Zheng, Y. X.; Dong, G.; He, L. Y.; Wu, G.; Zheng, H. D.; Deng, C. L. In Vitro Study of Calcium Phosphate Layers on Hydroxyapatite Ceramics Surface Mineralized in Different Solutions. *Ceram. Int.* **2016**, *42*, 1660−1665.
(38) Gong, L.; Zha, J.; Pan, L.; Ma, C.; He, Y.-C. Highly Efficient Conversion of Sunflower Stalk-Hydrolysate to Furfural by Sunflower Stalk Residue-Derived Carbonaceous Solid Acid in Deep Eutectic Solvent/Organic Solvent System. *Bioresour. Technol.* **2022**, *351*, No. 126945.
(39) Wang, X. Q.; Qiu, M.; Tang, Y. W.; Yang, J. R.; Shen, F.; Qi, X. H.; Yu, Y. L. Synthesis of Sulfonated Lignin-Derived Ordered Mesoporous Carbon for Catalytic Production of Furfural from Xylose. *Int. J. Biol. Macromol.* **2021**, *187*, 232−239.
(40) Beyene, D.; Chae, M.; Vasanthan, T.; Bressler, D. C. A Biorefinery Strategy That Introduces Hydrothermal Treatment Prior to Acid Hydrolysis for Co-Generation of Furfural and Cellulose Nanocrystals. *Front. Chem.* **2020**, *8*, 323.
(41) Ogundowo, O.; Ibrahim, H. Promising Sulfonated Carbon-Based Zirconia Catalyst for Renewable Furfural Production. *Biomass Convers. Biorefin.* **2022**, DOI: 10.1007/s13399-022-03071-2.
(42) Li, H. L.; Ren, J. L.; Zhong, L. J.; Sun, R. C.; Liang, L. Production of Furfural from Xylose, Water-Insoluble Hemicelluloses and Water-Soluble Fraction of Corncob via a Tin-Loaded Montmorillonite Solid Acid Catalyst. *Bioresour. Technol.* **2015**, *176*, 242−248.
(43) Rasmussen, H.; Sorensen, H. R.; Meyer, A. S. Formation of Degradation Compounds from Lignocellulosic Biomass in the Biorefinery: Sugar Reaction Mechanisms. *Carbohydr. Res.* **2014**, *385*, 45−57.
(44) Kumar, R.; Prakash, K. H.; Cheang, P.; Khor, K. A. Temperature Driven Morphological Changes of Chemically Precipitated Hydroxyapatite Nanoparticles. *Langmuir* **2004**, *20*, 5196−5200.
(45) Tang, S. Q.; Fei, X. C. Refractory Calcium Phosphate-Derived Phosphorus Fertilizer Based on Hydroxyapatite Nanoparticles for Nutrient Delivery. *ACS Appl. Nano Mater.* **2021**, *4*, 1364−1376.
(46) Wang, D. J.; Xie, Y. S.; Jaisi, D. P.; Jin, Y. Effects of Low-Molecular-Weight Organic Acids on the Dissolution of Hydroxyapatite Nanoparticles. *Environ. Sci.: Nano* **2016**, *3*, 768−779.
(47) Liu, J.; Liu, H. T.; Chen, L.; An, Y. Z.; Jin, X.; Li, X. X.; Liu, Z.; Wang, G. H.; Liu, R. Study on the Removal of Lignin from Pre-Hydrolysis Liquor by Laccase-Induced Polymerization and the Conversion of Xylose to Furfural. *Green Chem.* **2022**, *24*, 1603−1614.
(48) Chen, W.; Westerhoff, P.; Leenheer, J. A.; Booksh, K. Fluorescence Excitation-Emission Matrix Regional Integration to Quantify Spectra for Dissolved Organic Matter. *Environ. Sci. Technol.* **2003**, *37*, 5701−5710.
(49) Zhang, J.; Ding, G.; Wang, Y.; Wang, F.; Wang, H.; Liu, Y.; Zhu, Y.; Li, Y. Regulation of Bronsted Acid Sites to Enhance the Decarburization of Hexoses to Furfural. *Catal. Sci. Technol.* **2022**, *12*, 3506−3515.
(50) He, O.; Zhang, Y.; Wang, P.; Liu, L.; Wang, Q.; Yang, N.; Li, W.; Champagne, P.; Yu, H. Experimental and Kinetic Study on the Production of Furfural and HMF from Glucose. *Catalysts* **2021**, *11*, 11.
(51) Gong, M.; Zhou, Z. L.; Liu, S. P.; Zhu, S. H.; Li, G. Q.; Zhong, F.; Mao, J. Formation Pathways and Precursors of Furfural during Zhenjiang Aromatic Vinegar Production. *Food Chem.* **2021**, *354*, No. 126945.
(52) Srivastava, R.; Bousquieres, J.; Cepeda-Vazquez, M.; Roux, S.; Bonazzi, C.; Rega, B. Kinetic Study of Furan and Furfural Generation during Baking of Cake Models. *Food Chem.* **2018**, *267*, 329−336.
(53) Matsagar, B. M.; Van Nguyen, C.; Hossain, M. S. A.; Islam, M. T.; Yamauchi, Y.; Dhepe, P. L.; Wu, K. C. W. Glucose Isomerization Catalyzed by Bone Char and the Selective Production of 5-Hydroxymethylfurfural in Aqueous Media. *Sustain. Energy Fuels* **2018**, *2*, 2148−2153.
(54) Nie, Y. F.; Hou, Q. D.; Bai, C. Y. L.; Qian, H. L.; Bai, X. Y.; Ju, M. T. Transformation of Carbohydrates to 5-Hydroxymethylfurfural with High Efficiency by Tandem Catalysis. *J. Clean. Prod.* **2020**, *274*, No. 123023.
(55) Ye, L.; Han, Y. W.; Wang, X. T.; Lu, X. B.; Qi, X. H.; Yu, H. B. Recent Progress in Furfural Production from Hemicellulose and Its Derivatives: Conversion Mechanism, Catalytic System Solvent Selection. *Mol. Catal.* **2021**, *515*, No. 111899.
(56) Lalander, C.; Nordberg, Å.; Vinnerås, B. A Comparison in Product-Value Potential in Four Treatment Strategies for Food Waste and Faeces − Assessing Composting, Fly Larvae Composting and Anaerobic Digestion. *GCB Bioenergy* **2018**, *10*, 84−91.
(57) Liu, T.; Zhang, Q.; Kang, X.; Hou, J.; Luo, T.; Zhang, Y. Household Food Waste to Biogas in Västerås, Sweden: A Comprehensive Case Study of Waste Valorization. *Sustainability* **2022**, *14*, 11925.
(58) Levstek, T.; Rozman, Č. A Model for Finding a Suitable Location for a Micro Biogas Plant Using Gis Tools. *Energies* **2022**, *15*, 7522.
(59) Barbera, E.; Bertucco, A.; Nigam, K. D. P.; Kumar, S. Techno-Economic Analysis of a Micro-Scale Biogas Plant Integrated with

https://doi.org/10.1021/acsomega.3c00762
ACS Omega 2023, 8, 18760−18772

Microalgae Cultivation for the Treatment of Organic Municipal Waste. *Chem. Eng. J.* **2022**, *450*, No. 138323.
(60) Naeiji, E.; Noorpoor, A.; Ghnavati, H. Increasing Biomethane Production in MSW Anaerobic Digestion Process by Chemical and Thermal Pretreatment and Process Commercialization Evaluation. *Fermentation* **2022**, *8*, 463.
(61) Al-Wahaibi, A.; Osman, A. I.; Al-Muhtaseb, A. H.; Alqaisi, O.; Baawain, M.; Fawzy, S.; Rooney, D. W. Techno-Economic Evaluation of Biogas Production from Food Waste via Anaerobic Digestion. *Sci. Rep.* **2020**, *10*, No. 15719.
(62) Chen, T.; Zhang, S.; Yuan, Z. Adoption of Solid Organic Waste Composting Products: A Critical Review. *J. Clean. Prod.* **2020**, *272*, No. 122712.
(63) Kim, M.-H.; Song, Y.-E.; Song, H.-B.; Kim, J.-W.; Hwang, S.-J. Evaluation of Food Waste Disposal Options by LCC Analysis from the Perspective of Global Warming: Jungnang Case, South Korea. *Waste Manage.* **2011**, *31*, 2112−2120.
(64) Lin, Z.; Ooi, J. K.; Woon, K. S. An Integrated Life Cycle Multi-Objective Optimization Model for Health-Environment-Economic Nexus in Food Waste Management Sector. *Sci. Total Environ.* **2022**, *816*, No. 151541.
(65) Al Mussa Ugak, M.; Mohamad, N. E.; Rajin, M.; Lamaming, J.; Saalah, S.; Yaser, A. Z. Passive Aerated In-Vessel Composting of Food Waste with the Addition of Sabah Ragi for Campus Sustainability: Mass Balance, Dwarf Crape Jasmine Growth and Techno-Economic Study. *J. Mater. Cycles Waste Manag.* **2023**, *25*, 899−909.
(66) Keng, Z. X.; Chong, S.; Ng, C. G.; Ridzuan, N. I.; Hanson, S.; Pan, G. T.; Lau, P. L.; Supramaniam, C. V.; Singh, A.; Chin, C. F.; Lam, H. L. Community-Scale Composting for Food Waste: A Life-Cycle Assessment-Supported Case Study. *J. Clean. Prod.* **2020**, *261*, No. 121220.
(67) Nguyen, T. T. X.; Tomberlin, J. K.; Vanlaerhoven, S. Ability of Black Soldier Fly (Diptera: Stratiomyidae) Larvae to Recycle Food Waste. *Environ. Entomol.* **2015**, *44*, 406−410.
(68) Cheng, J. Y. K.; Lo, I. M. C. Investigation of the Available Technologies and Their Feasibility for the Conversion of Food Waste into Fish Feed in Hong Kong. *Environ. Sci. Pollut. Res.* **2016**, *23*, 7169−7177.
(69) Salomone, R.; Saija, G.; Mondello, G.; Giannetto, A.; Fasulo, S.; Savastano, D. Environmental Impact of Food Waste Bioconversion by Insects: Application of Life Cycle Assessment to Process Using Hermetia Illucens. *J. Clean. Prod.* **2017**, *140*, 890−905.
(70) Ferrer Llagostera, P.; Kallas, Z.; Reig, L.; Amores de Gea, D. The Use of Insect Meal as a Sustainable Feeding Alternative in Aquaculture: Current Situation, Spanish Consumers' Perceptions and Willingness to Pay. *J. Clean. Prod.* **2019**, *229*, 10−21.
(71) Jagtap, S.; Garcia-Garcia, G.; Duong, L.; Swainson, M.; Martindale, W. Codesign of Food System and Circular Economy Approaches for the Development of Livestock Feeds from Insect Larvae. *Foods* **2021**, *10*, 1701.
(72) Ravi, H. K.; Degrou, A.; Costil, J.; Trespeuch, C.; Chemat, F.; Vian, M. A. Larvae Mediated Valorization of Industrial, Agriculture and Food Wastes: Biorefinery Concept through Bioconversion, Processes, Procedures, and Products. *Processes* **2020**, *8*, 857.
(73) Sangeetha, B.; Mohana Priya, S.; Pravin, R.; Tamilarasan, K.; Baskar, G. Process Optimization and Technoeconomic Assessment of Biodiesel Production by One-Pot Transesterification of Ricinus Communis Seed Oil. *Bioresour. Technol.* **2023**, *376*, No. 128880.
(74) Dougher, M.; Soh, L.; Bala, A. M. Techno-Economic Analysis of Interesterification for Biodiesel Production. *Energy Fuels* **2023**, *37*, 2912−2925.
(75) Hamed, S. M.; El Shimi, H. I.; van Dijk, J. R.; Osman, A. I.; Korany, S. M.; AbdElgawad, H. A Novel Integrated System for Heavy Metals Removal and Biodiesel Production via Green Microalgae: A Techno-Economic Feasibility Assessment. *J. Environ. Chem. Eng.* **2022**, *10*, No. 108804.
(76) Zheng, L.; Hou, Y.; Li, W.; Yang, S.; Li, Q.; Yu, Z. Biodiesel Production from Rice Straw and Restaurant Waste Employing Black Soldier Fly Assisted by Microbes. *Energy* **2012**, *47*, 225−229.
(77) Elsayed, M.; Ran, Y.; Ai, P.; Azab, M.; Mansour, A.; Jin, K.; Zhang, Y.; Abomohra, A. E.-F. Innovative Integrated Approach of Biofuel Production from Agricultural Wastes by Anaerobic Digestion and Black Soldier Fly Larvae. *J. Clean. Prod.* **2020**, *263*, No. 121495.
(78) Ntimbani, R. N.; Farzad, S.; Görgens, J. F. Techno-Economics of One-Stage and Two-Stage Furfural Production Integrated with Ethanol Co-Production from Sugarcane Lignocelluloses. *Biofuel. Bioprod. Biorefin.* **2021**, *15*, 1900−1911.
(79) Meng, Y.; Zhou, Y.; Shao, Y.; Zhou, D.; Shen, D.; Long, Y. Evaluating the Potential of the Microwave Hydrothermal Method for Valorizing Food Waste by Producing 5-Hydroxymethylfurfural. *Fuel* **2021**, *306*, No. 121769.
(80) Xiao, L.; Meng, Y.; Jin, H.; Wang, Y.; Fan, L.; Shen, D.; Long, Y. Conversion of Waste-Activated Sludge from Wastewater Treatment Plants to 5-Hydroxymethylfurfural by Microwave Hydrothermal Treatment. *Biomass Convers. Biorefin.* **2022**, DOI: 10.1007/s13399-022-03076-x.
(81) Wiranarongkorn, K.; Im-orb, K.; Patcharavorachot, Y.; Maréchal, F.; Arpornwichanop, A. Comparative Techno-Economic and Energy Analyses of Integrated Biorefinery Processes of Furfural and 5-Hydroxymethylfurfural from Biomass Residue. *Renew. Sustain. Energy Rev.* **2023**, *175*, No. 113146.
(82) Almeida, S. G. C.; Mello, G. F.; Kovacs, T. K.; Silva, D. D. V.; Costa, M. A. M.; Dussán, K. J. Furfural Production through Two Bioconversion Routes: Experimental Optimization and Process Simulation. *Waste Biomass Valor.* **2022**, *13*, 4013−4025.
(83) Saadoun, J. H.; Montevecchi, G.; Zanasi, L.; Bortolini, S.; Macavei, L. I.; Masino, F.; Maistrello, L.; Antonelli, A. Lipid Profile and Growth of Black Soldier Flies (Hermetia Illucens, Stratiomyidae) Reared on By-Products from Different Food Chains. *J. Sci. Food Agric.* **2020**, *100*, 3648−3657.

https://doi.org/10.1021/acsomega.3c00762
ACS Omega 2023, 8, 18760−18772